The ground state of the two-leg Hubbard ladder
A density-matrix renormalization group study

R.M. Noack [a,*], S.R. White [b], D.J. Scalapino [c]

[a] Institut für Theoretische Physik, Universität Würzburg, Am Hubland, 97074 Würzburg, Germany
[b] Department of Physics and Astronomy, University of California, Irvine, CA 92717, USA
[c] Department of Physics, University of California, Santa Barbara, CA 93106, USA

Abstract

We present density-matrix renormalization group results for the ground state properties of two-leg Hubbard ladders. The half-filled Hubbard ladder is an insulating spin-gapped system, exhibiting a crossover from a spin liquid to a band insulator as a function of the interchain hopping matrix element. When the system is doped, there is a parameter range in which the spin gap remains. In this phase, the doped holes form singlet pairs and the pair field and the "$4k_F$" density correlations associated with pair-density fluctuations decay as power laws, while the "$2k_F$" charge density wave correlations decay exponentially. We discuss the behavior of the exponents of the pairing and density correlations within this spin-gapped phase. Additional one-band Luttinger liquid phases which occur in the large interband hopping regime are also discussed.

PACS: 71.20.-b; 75.10.Lp; 75.40.Gb

1. Introduction

There are a number of new materials which contain weakly coupled arrays of metal–oxide ladders. For example, $SrCu_2O_3$ [1] and $La_2Cu_2O_5$ [2,3] contain two-leg ladders with Cu–O–Cu rungs, and $(VO)_2P_2O_7$ [4] contains isolated two-leg V–O ladders. Alternatively, $Sr_2Cu_3O_5$ contains three-leg ladders and $Sr_nCu_{n+1}O_{2n+1}$ has $n + 1$-leg ladders [1]. Magnetic-susceptibility and nuclear relaxation time measurements provide evidence [5] that in the insulating state, the even-leg ladders have a spin gap while the odd-leg ladders have gapless spin excitations. It is of great interest to understand what happens when holes are doped into these systems, and, in particular, what happens when holes are doped into the spin-gapped two-leg ladders. Recently, Hiroi and Takano [6] reported that the two-leg ladder compound $La_2Cu_2O_5$ could be hole-doped by substituting Sr for some of the La. They found that the conductivity of the doped ladders has a metallic behavior and that magnetic susceptibility data suggests that a spin gap remains in the lightly doped system.

Here we examine the properties of a Hubbard model on a two-chain ladder in order to understand the ground state-behavior of the undoped and doped two-leg ladders in terms of an itinerant electron model. We will show primarily numerical results for the energies and equal-time correlations of the ground and low-lying states obtained using the density-matrix renormalization group technique [7] (DMRG). While

* Corresponding author. Fax: +49 931 888 5141;
e-mail: reinhard@physik.uni-wuerzburg.de.

parts of this work have been published previously [8], here we will discuss the results in more detail, make comparisons to weak- and strong-coupling analytic pictures, and also present some new results on the local structure of the pairing, the "$4k_F$" charge-density wave (CDW), and on the behavior of the spin and charge gaps in the quarter-filled system.

The Hubbard and related models on a two-leg ladder have received much theoretical attention recently, via various analytic approximations, as well as a variety of numerical techniques. We direct the reader to a recent review [9] and the references contained therein. Previous numerical work includes Lanczos calculations for a t–J model by Dagotto et al. [10] who suggested that antiferromagnetic $S = \frac{1}{2}$ coupled chains should have a spin gap and that if the two-chain system could be doped, it would have enhanced superconducting or charge-density wave correlations in the ground state. In Ref. [11] the Heisenberg model was treated using exact diagonalization and analytic techniques in order to determine the ground-state properties, the temperature dependence of the spin susceptibility, and the spin excitation spectrum. Rice et al. [12,13] discussed a t–J model and suggested that if this system were lightly doped, the spin-gap phase would persist and a ground state with dominant superconducting correlations could be realized. The one- and two-particle dynamical correlation functions were calculated for the half-filled Hubbard ladder using quantum Monte Carlo and a maximum entropy analytic continuation in Ref. [14] There have also been a number of weak-coupling renormalization group calculations [15–20] which find evidence for a variety of phases. We will discuss the results of one of these calculations [20] in more detail below and compare them to our numerical calculations.

In the following, we present numerical evidence that indicates that the half-filled two-leg Hubbard ladder is a spin-gapped insulator for all non-zero values of the Coulomb interaction U, and the interchain coupling $t_\perp$. We show that for weak U, there is a well-defined spin-liquid insulator to band insulator transition that corresponds to the $U = 0$ one-band to two-band transition. For stronger U, this transition evolves into a smooth crossover. When the system is doped, the charge gap disappears, but the spin gap remains for a range of $t_\perp$ associated with overlapping bonding and antibonding bands. For $t_\perp$ larger than this range,

the numerical results are consistent with Luttinger liquid behavior. Within the spin-gap phase, we show that there is an attractive pairing interaction, a d wave-like structure of the pair wave function, and algebraically decaying pairing and "$4k_F$" CDW correlations. However, the CDW correlations do not seem to decay in the manner predicted by weak-coupling bosonization treatments of the system [21,20].

The organization of the paper is as follows: in Section 2, we review the basic properties of the model and discuss the predictions of weak-coupling renormalization group and bosonization calculations. In Section 2.1, we exhibit numerical results for the half-filled system, discuss the properties of the spin liquid state and the crossover to a band insulator as a function of the perpendicular hopping. In Section 2.2, we explore the effects of doping holes into the system, and discuss the phases present as a function of the perpendicular hopping at various fillings. We discuss in detail the behavior of the holes within the gapped spin liquid state that persists as the isotropic system is doped.

2. The two-chain Hubbard model

The single band Hubbard model on two coupled chains of length L has the Hamiltonian

$$H = -t \sum_{i,\lambda\sigma} (c^\dagger_{i,\lambda\sigma} c_{i+1,\lambda\sigma} + \text{h.c.})$$
$$-t_\perp \sum_{i,\sigma} (c^\dagger_{i,1\sigma} c_{i,2\sigma} + \text{h.c.}) + U \sum_{i\lambda} n_{i,\lambda\uparrow} n_{i,\lambda\downarrow}.$$

$$(1)$$

Here $c^\dagger_{i,\lambda\sigma}$ and $c_{i,\lambda\sigma}$ create and destroy, respectively, an electron on rung i and chain λ with spin σ, and $n_{i,\lambda\sigma} = c^\dagger_{i,\lambda\sigma} c_{i,\lambda\sigma}$. We will also use the notation $n_{i,\lambda} \equiv \sum_\sigma n_{i,\lambda\sigma}$. The hopping integral parallel to the chains is t, the hopping between the chains $t_\perp$, and U is the on-site Coulomb interaction. For the remainder of this work, we set $t = 1$ and measure all energies in units of t. Within this paper, we will discuss a system with open boundary conditions both between the two chains and at the ends of the chains. In other words, site $i, 1$ is connected through only one hopping term to site $i, 2$, and site $1, \lambda$ is not directly connected to site L, λ.

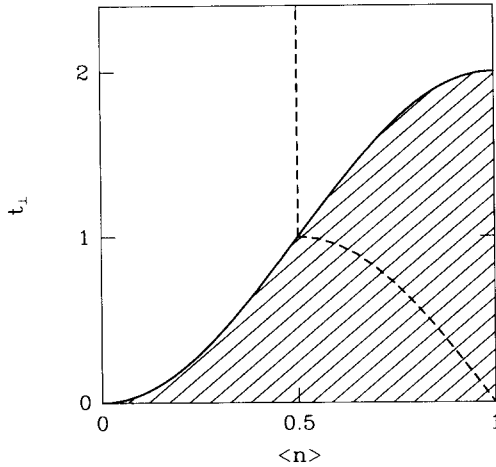The non-interacting, $U = 0$, Hamiltonian can be diagonalized by writing the hopping term in terms of

Fig. 1. The $\langle n \rangle$–$t_\perp$ phase diagram for the $U = 0$ system. In the shaded region, both the bonding (lower) and antibonding (upper) bands are occupied. At the solid line, the lowest part of the antibonding band just touches the Fermi surface, and on the dashed line, the bonding band is half-filled.

bonding and antibonding states on a rung and Fourier transforming parallel to the chains. The energy for the infinite two-chain system is then given by

$$\varepsilon_k = -(2t \cos k + t_\perp \cos k_\perp),\qquad (2)$$

with $k = (k, k_\perp)$, where $k_\perp = 0$ and $k_\perp = \pi$ corresponds to the energy of the bonding and antibonding band, respectively, and k is the momentum along the chains. For $t_\perp = 0$, the two bands will be degenerate, and for nonzero $t_\perp$, they will be separated by an energy $2t_\perp$.

Due to the band structure, the $U = 0$ phase diagram in the $t_\perp$–$\langle n \rangle$ plane, shown in Fig. 1, exhibits significant structure. Both bands will be occupied when $t_\perp < t_{\perp c}$ (shaded region), whereas when $t_\perp > t_{\perp c}$, only the bonding band will be occupied. Here $t_{\perp c} = 1 - \cos \pi \langle n \rangle$ and is shown by a solid line and $\langle n \rangle \equiv \langle \sum_\sigma c_{i,\lambda,\sigma}^\dagger c_{i,\lambda,\sigma} \rangle$ is the band filling. At half-filling $t_{\perp c} = 2$, and the system is a two-band metal for $t_\perp < 2$ and a band insulator with a completely occupied bonding band for $t_\perp > 2$.

Along the dashed line in Fig. 1, the bonding band is half-filled. At half-filling ($\langle n \rangle = 1$), this occurs at $t_\perp = 0$, where both bands are half-filled. As $\langle n \rangle$ is reduced, the $t_\perp$ at which the bonding band is half-filled becomes larger and the occupation of the antibonding band at this point becomes smaller. When $\langle n \rangle = 0.5$,

the bonding band is half-filled only when the antibonding band is completely unoccupied, i.e. for $t_\perp > t_{\perp c}$.

Starting from the band-structure of the noninteracting system, one can treat the system within a weak-coupling picture by linearizing the band structure around the Fermi points and taking the continuum limit. The resulting model can be treated within a renormalization group or within a bosonization picture. Balents and Fisher [20] treated the small U, but arbitrary $t_\perp$ limit in a systematic, controlled procedure. In this approach, weak-coupling RG equations were numerically integrated for each value of $\langle n \rangle$ and $t_\perp$, evolving from infinitesimal U to small, but finite U. At this point bosonization methods were used to analyze the resulting hamiltonians. Their weak-coupling results for the phase diagram agree surprisingly well with our results at rather strong coupling. For this reason we will adopt their notation and compare our results with the results of their approach, which we will denote BFRG. An alternative strong-coupling approach, which is less predictive but perhaps more intuitive, is based on a short-range resonating-valence-bond variational ansatz [24,23]. This approach works particularly well in explaining the structure of the pair wavefunction in the doped, spin-gapped phase. We will discuss this in more detail in Section 2.2.

Since, in a weak-coupling picture such as that used by Balents and Fisher, there are in the general case four Fermi points (at $\pm k_F^b$ and $\pm k_F^a$), a bosonization treatment yields four possible modes: two spin modes, one symmetric and one antisymmetric with respect to interchange of the chains, and two charge modes, one symmetric and one antisymmetric. This is a generalization of the bosonization picture for the one-dimensional Luttinger model, which results in one spin and one charge mode. In general, each of the four modes can either be massive (i.e. gapped), or massless (with gapless excitations). Balents and Fisher classify the possible phases according to the number of massless charge modes n_c and spin modes n_s, using a notation Cn_cSn_s. In the two-chain system, there are nine possible phases, ranging from a C0S0 phase with excitation gaps in all four modes to a C2S2 phase, with all four modes gapless. For example, the two-chain analog of a Fermi liquid is a C2S2 phase, which occurs at $U = 0$ when both bands are partially filled. The BFRG calculation, which is valid for weak U but

arbitrary $t_\perp$, finds seven different ground-state phases in the $\langle n \rangle$–$t_\perp$ phase diagram.

Since the origin of the BFRG phases can be understood qualitatively in the context of the $U = 0$ phase diagram, we will briefly describe them here. At half-filling, the system is in a C0S0 (i.e. spin and charge gapped) phase for all $U > 0$ and $t_\perp > 0$. For $t_\perp < 2.0$, umklapp processes involving two particles scattering between the Fermi points lead to gaps opening in all four modes, producing a spin-liquid insulator. For $t_\perp > 2.0$, the system is a band insulator, as in the $U = 0$ case. Upon hole doping for $t_\perp > t_{\perp c}$, only the bonding band comes into play and the behavior is that of a one-band Luttinger liquid. Within this phase, there are gapless spin and charge modes, i.e. a C1S1 phase, except at quarter-filling, where the relevant bonding band is half-filled and umklapp processes within the band lead to a charge-gapped C0S1 phase. For $t_\perp < t_{\perp c}$ and $\langle n \rangle < 1$, the BFRG yields a C1S0 phase for most of the phase diagram. This phase, a spin liquid with one gapless symmetric charge mode, was also predicted by other, earlier weak-coupling renormalization group calculations [18,19], by various strong-coupling pictures [12,22,23], and has been found within the Hubbard and t–J models by numerical calculations [10,13,8,25]. Other phases are found in certain regions where special processes become relevant. One such region is in the vicinity of $t_\perp = t_{\perp c}$, where the bottom of the antibonding band just touches the Fermi surface so that its dispersion must be treated quadratically, rather than linearized. Here the BFRG calculation finds a C1S0 phase on the band-transition line. For $t_\perp$ slightly below $t_{\perp c}$, the Fermi velocities in the bands are quite different and the BFRG finds narrow regions of first C2S2, then C2S1 phases as $t_\perp$ is reduced. Umklapp processes become relevant where the bonding band is half-filled, along the dashed line in Fig. 1. Here the BFRG calculation finds a C1S2 phase along this line near half-filling and near quarter-filling, with an intermediate region in which the C1S0 phase remains present.

It is interesting at this point to compare the behavior of the two-chain system to that of the one-dimensional interacting electron gas (the 1D Hubbard model, for example). For repulsive short-range interactions, the 1D electron gas is a Luttinger liquid [26]. A Luttinger liquid has gapless spin and charge excitations (a C1S1 phase), except when umklapp processes be-

come relevant. The dominant long-distance behavior of the spin–spin, density–density, and on-site s wave correlation functions is power-law decay, and to leading order is [16]

$$\langle S(r) \cdot S(0) \rangle_{TL} = r^{-(1+K_\rho)} \cos(2k_F r),$$
$$\langle n(r) n(0) \rangle_{TL} = r^{-(1+K_\rho)} \cos(2k_F r),$$
$$\langle \Delta_s(r) \Delta_s^\dagger(0) \rangle_{TL} = r^{-(1+1/K_\rho)}, \qquad (3)$$

where $S(r)$ is the total spin at site r, $n(r)$ is the electron density, and $\Delta_s^\dagger(r)$ creates an on-site s-wave pair. The exponent K_ρ is a non-universal parameter dependent on the system parameters. There are logarithmic corrections multiplying these expressions which have been left out for simplicity. Umklapp processes become relevant at half-filling for the Hubbard model, at which point a charge gap develops, leading to a C0S1 mode. The strong-coupling limit of the half-filled Hubbard model is the Heisenberg model which has no charge degrees of freedom, and in 1D is known to have gapless spin excitations. The spin-spin correlation decays to leading order as [27]

$$\langle S(r) \cdot S(0) \rangle_{Heis} = r^{-1} \cos(\pi r). \qquad (4)$$

In the half-filled Hubbard model, the spin–spin correlation has this form and other correlation functions decay exponentially. According to the BFRG calculation, the doped two-chain system should behave as a Luttinger liquid when $t_\perp > t_{\perp c}$, and the filling of the Luttinger liquid corresponds to the filling of the bonding band. Therefore, the correlation functions should decay as power laws governed by one exponent, as in Eq. (3) in this regime, and by Eq. (4) at quarter-filling.

For attractive short-range interactions, the 1D electron gas falls into the Luther–Emery universality class [28]. Within the Luther–Emery model, there is a spin gap and one low-lying charge mode (C1S0). The s wave pairing correlation function and the CDW correlation function both decay algebraically, with a power parameterized by the CDW exponent K_ρ. The leading behavior of these two correlation function is given by

$$\langle n(r) n(0) \rangle_{LE} = r^{-K_\rho} \cos(2k_F r),$$
$$\langle \Delta_s(r) \Delta_s^\dagger(0) \rangle_{LE} = r^{-1/K_\rho}. \qquad (5)$$

Here K_ρ is also dependent on the model parameters, such as the band-filling, or the strength of the

Coulomb interaction, $|U|$, in the attractive Hubbard model. Within the BFRG calculation, the doped two-leg ladder falls into a Luther–Emery-like C1S0 phase for much of the region for $t_\perp < t_{\perp c}$. It is therefore a relevant question whether there are correlations analogous to those in Eq. (5) with a reciprocal relation between the exponents in this phase. Bosonization treatments of the two-chain system predict [21,20] that the relevant CDW operator will occur at the "$4k_F$" wave vector $q^* = (2[k_F^b + k_F^a], 0)$ with an effective density operator $n_i^{eff} = n_{i,1} n_{i,2}$, and that the pair wave function will no longer be s wave, but d wave-like with the largest amplitude across a rung. Since the behavior of the correlation functions is dependent on the parameter K_ρ, which is a non-universal quantity which can depend on the parameters of the model, it is important to determine the exponents within a particular phase. The least restrictive criterium for the superconducting pairing being dominant over the CDW is that the correlation function decays more slowly at long distances, which occurs when $K_\rho > 1$. However, the consideration of the effects of impurity scattering and crossover to three dimensions [29] can lead one to the more stringent requirement that $K_\rho > 3$, in order to obtain a stable superconducting state.

The numerical results shown in this work are all calculated using the DMRG technique [7] on finite lattices of 2×8 to 2×64 sites. We obtain the energies and equal-time correlation functions of the ground state and the low-lying excited states of the finite cluster. While the DMRG technique gives energies that are, in principle, variational, it has proven to give quite accurate results for 1D quantum lattice systems. The method provides a controlled way of numerically diagonalizing a finite system within a truncated Hilbert space, by successively building up part of the system using a real-space blocking transformation, and then using the reduced density matrix to truncate the Hilbert space of that part of the system in a controlled way. One can increase the accuracy by increasing the number of states kept, and can examine the convergence with the number of states. Here we typically keep 400 states per block, although in the numerically more difficult cases, such as the calculation of the spin gap on doped 2×32 lattices with small $t_\perp$, we keep up to 550 states. Truncation errors, given by the sum of the density matrix eigenvalues of the discarded states, vary from 3.7×10^{-5} in the worse case to $O(10^{-8})$ in the best cases. This discarded density-matrix weight is directly correlated with the absolute error in the energy [7]. It was only possible to obtain accurate calculations on the larger lattice sizes, 2×40 and 2×64, in certain parameter regimes, in which the convergence with the number of states was relatively rapid. In other regimes, the largest lattice size was 2×32. We estimate that the maximum errors on the quantities shown in this paper are at most a few percent and typically are of the order of the plotting symbol size or less. We apply open boundary conditions to the lattice because the DMRG method is most accurate for a given amount of computational effort with these boundary conditions.

2.1. Half-filling

As discussed above, the undoped two-leg ladder materials are gapped spin-liquid insulators. Analytic and numerical studies of the Heisenberg model, which is the strong-coupling limit of the Hubbard model at half-filling, determine that the system is a spin-liquid insulator for isotropic couplings [10,11,22]. There is also numerical evidence that this spin-liquid state is present for *all* ratios of the interchain to intrachain coupling [11,23,30]. However, it is not clear how the crossover from the weak-coupling picture dominated by the band-structure effects to the strong-coupling spin-liquid state takes place within the Hubbard model. We will explore this question in this section.

In order to see the structure of the correlations at half-filling, we first examine the spin-spin correlation function defined as

$$S(i, j, \lambda) = \langle M_{i,\lambda}^z M_{j,1}^z \rangle, \qquad (6)$$

where $M_{i,\lambda}^z = n_{i,\lambda\uparrow} - n_{i,\lambda\downarrow}$ is the z component of the on-site magnetization. This correlation function, multiplied by a factor $(-1)^i$ which removes the antiferromagnetic $q = \pi$ structure, is shown in Fig. 2 on a semilog scale. Since the correlation functions are straight lines on the semilog plot, the decay is exponential, as we would expect in a gapped spin liquid. The spin–spin correlation function decays more rapidly as U is increased, implying the correlation length decreases with U. The behavior of the correlation length, obtained by fitting a straight line to the
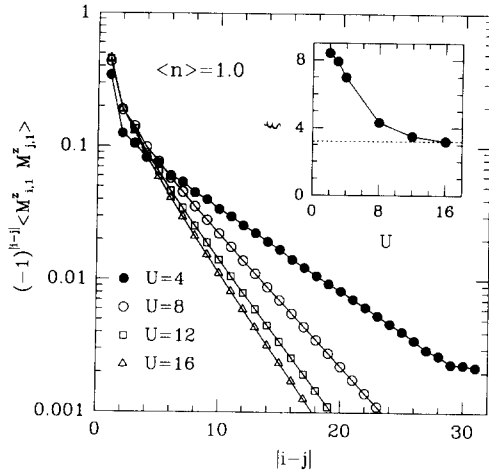
Fig. 2. The spin–spin correlation function $(-1)^\ell \langle M^z_{i,\lambda} M^z_{j,1} \rangle$ for various U at half-filling ($\langle n \rangle = 1.0$) plotted on a semilog scale. The inset shows the correlation length extracted from the slope of the lines as a function of U, with the dashed line the Heisenberg value from Ref. [23].
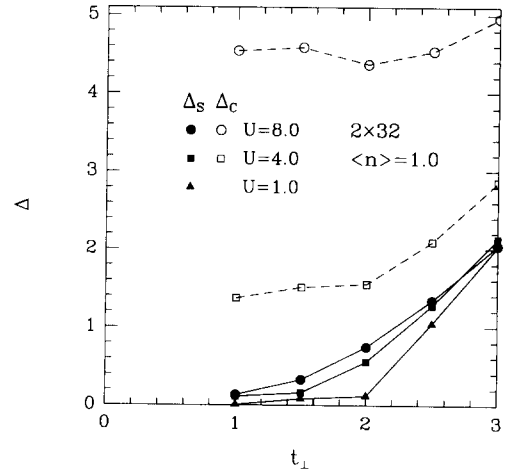

Fig. 3. The spin gap Δ_s and the charge gap Δ_c as a function of $t_\perp$ at half-filling on a 2×32 lattice for various U.

curves between 6 and 19 lattice spacings, is shown in the inset. The dashed line in the inset is the spin correlation length for the two-chain isotropic Heisenberg system, $\xi = 3.19$, taken from Ref. [23]. As can be seen, the correlation length for the Hubbard model converges to the Heisenberg value for large U, as one would expect.

We have examined the spin–spin correlation function for a variety of U and $t_\perp$ at half-filling, down to $t_\perp = 0.2$ at $U = 1$, and $U = 0.5$ at $t_\perp = 1.0$. The decay of the correlation functions is consistent with exponential decay and a finite correlation length at half-filling for all $t_\perp$ and U we have examined. Therefore, we believe the spin liquid phase is present at all $t_\perp$ and U at half-filling. This is consistent with weak-coupling renormalization group treatments [19,20].

We have also examined other correlation functions, such as the density–density and pair correlation functions, for the half-filled system. In all cases they also decay exponentially, with a correlation length shorter than that of the spin–spin correlation function.

We next consider the charge and spin gaps defined by

$$\Delta_c = \tfrac{1}{2}[E_0(N-1, N-1)$$
$$+ E_0(N+1, N+1) - 2E_0(N,N)] \qquad (7)$$

and

$$\Delta_s = E_0(N+1, N-1) - E_0(N,N), \qquad (8)$$

respectively. Here $E_0(N_\uparrow, N_\downarrow)$ is the ground state energy for $N_\uparrow$ spin-up electrons and $N_\downarrow$ spin-down electrons. Since our current DMRG program cannot target states of a particular transverse symmetry, we can only calculate the gaps to the lowest-lying spin and charge excited states, irrespective of symmetry. We show spin and charge gaps for a range of U and $t_\perp$ in Fig. 3. For $U = 0$, the system is a two-band metal, as discussed in Section 2, for $t_\perp < 2$, and a band insulator for $t_\perp > 2$. Therefore, for $U = 0$ both gaps would be zero for $t_\perp < 2$, and would be set by the band separation $2(t_\perp - 1)$ for $t_\perp > 2$. For the $U = 1$ spin gap in Fig. 3, the behavior for $t_\perp > 2$ follows the $U = 0$ form. However, for $t_\perp < 2$, we expect a nonvanishing spin gap due to the spin-liquid state, consistent with the exponentially decaying spin–spin correlation function. We find numerically that the gap in this region is finite, but relatively small, with its size associated with the strength of the antiferromagnetic correlations in the spin-liquid state. We calculate the spin gap over a limited range of $t_\perp$ because the numerical accuracy of the DMRG method and the size of the spin gap both become smaller with lower $t_\perp$. Since one needs to calculate small energy differences and do finite size scaling in order to accurately determine the spin gap, we find that an examination of the ground-state spin–spin correlations, discussed above, is a more sensitive
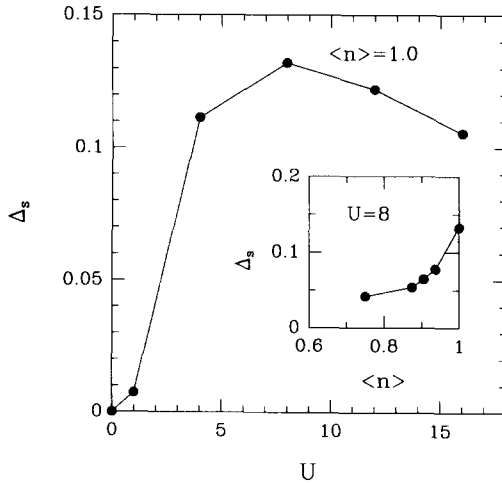
Fig. 4. The spin gap Δ_s as a function of U at half-filling on a 2×32 lattice. The inset shows Δ_s as a function of filling for $U = 8$.

test for the existence of the spin-liquid state, given a particular numerical accuracy. We omit the charge gap for $U = 1$ because the accuracy of the calculated charge gap is comparable to its size in this region.

As U is increased, the relatively sharp transition from a spin liquid insulator to a band insulator becomes a smooth crossover. This can be understood in terms of the spin gap because in the Heisenberg limit, the size of the spin gap is set by the perpendicular coupling $J_\perp \approx 4t_\perp^2/U$ for large $J_\perp$. One can see the crossover to this behavior for $U = 4$ and 8, and intermediate $t_\perp$. However, as $t_\perp$ becomes larger, the Heisenberg mapping breaks down (when $4t_\perp^2$ is of the order of U), and the linear growth in $t_\perp$ characteristic of the band insulator is restored. For large U, $\Delta_c \approx U/2$ at half-filling, and we can see that the charge gap is approximately this size for $U = 4$ and 8. For $U = 4$, the crossover to linear growth of the charge gap with $t_\perp$ is visible for $t_\perp > 2$.

We examine the dependence of the spin gap on U at half-filling for the isotropic ladder ($t_\perp = 1.0$) in Fig. 4. For small U, the spin gap increases with U as one might expect from a weak-coupling picture. For very large U, the spin gap should scale with $J \approx 4t^2/U$, since J is the only energy scale in the Heisenberg system. Therefore, the spin gap will have a peak at some intermediate U, seen to be approximately $U = 8$ in Fig. 4.

Therefore, at half-filling, the two-leg Hubbard ladder is an insulator with a spin and charge gap for all U

and $t_\perp$, with a crossover from a spin-liquid insulator to a band insulator at $t_{\perp c} = 2.0$ that grows less sharp as U increases.

2.2. The doped system

The evolution of the spin-liquid state of the half-filled system with doping is a quite interesting question. As discussed above, weak-coupling treatments such as the BFRG described above make rather specific predictions about the phase diagram of the doped system. In particular, it is expected that when the isotropic system is doped, the spin gap will remain, there will be one low-lying charge mode, and that there will be pairing of the charge carriers. In addition, according to the BFRG picture, there will a set of phase transitions associated with the weak-coupling one-band to two-band transition, and with the umklapp processes that occur when one of the bands is half-filled. It is not clear to what extent this picture will hold within a Hubbard model on a lattice and with a realistic band structure, or at the relatively strong coupling, $U = 8$, treated here. The detailed properties of the system within each phase, such as the non-universal exponents that determine the relative strength of various correlation functions, have not yet been calculated in detail using weak-coupling methods and are thus interesting to determine.

One can also approach the behavior of this system from a strong coupling point of view. This has been done within the t–J model by starting from the limit of strong magnetic coupling between the chains [12], $J_\perp \gg J$. One can then treat the interactions between the rungs perturbatively, and, for small doping, make states that are delocalized products of simple excitations of the rungs. This gives a physical picture of the behavior for a low density of holes, and predicts pairing. In Ref. [13] it is then argued that the behavior at isotropic coupling is continuously connected to that at large $J_\perp$ by showing that, within exact diagonalization calculations, there is a continuous evolution of the properties with $J_\perp$, and a qualitative correspondence between the large $J_\perp$ case and the isotropic case. A variational dimer resonating-valence-bond (RVB) state [23] used to treat the Heisenberg ladder gives a qualitatively similar picture, and helps justify the continuity between small and large $J_\perp$. In the following, we will examine the properties of the model as a func-
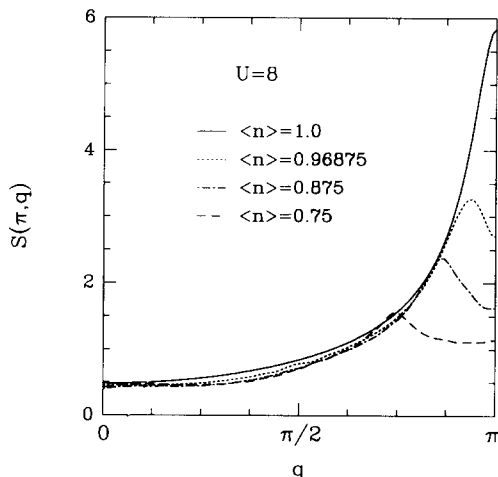
Fig. 5. The continuous Fourier transform $S(q, \pi)$ of the spin–spin correlation function $S(i, j, \lambda)$ for $U = 8$ at various fillings on a 2×32 lattice.

tion of filling, and then take slices through the phase diagram at constant $\langle n \rangle$ and varying $t_\perp$ at two fillings: $\langle n \rangle = 0.875$ and $\langle n \rangle = 0.5$ (quarter filling).

We first examine the behavior of the spin gap and the spin–spin correlation function when the half-filled system with isotropic coupling ($t_\perp = 1.0$) is doped with holes. Upon doping, the spin gap, as shown in the inset of Fig. 4 for a 2×32 lattice, is reduced but remains finite down to a filling of at least $\langle n \rangle = 0.75$. Although these results are calculated on a finite lattice, we will examine the behavior as a function of system size and extrapolate to the thermodynamic limit at particular fillings below. In the regime shown in the inset of Fig. 4, the spin gap remains finite in the thermodynamic limit.

The Fourier transform of the $q = (q, \pi)$ branch of the spin–spin correlation function is shown in Fig. 5 for fillings between $\langle n \rangle = 0.75$ and $\langle n \rangle = 1.0$. In order to reduce the effects of the broken translational invariance due to the open boundary conditions, we average the spin–spin correlation function over up to six i, j pairs for each $|i - j|$ in real space before Fourier transforming. A continuous range of frequencies is shown because the correlation function decayed sufficiently rapidly so that we could obtain its value for all non-negligible separations. Thus the actual lattice size used in the calculation is irrelevant, and unlike the usual treatment of a finite system with periodic boundary conditions, a straightforward Fourier transform yields

valid results at any frequency value, provided that the correlation function is assumed to vanish at larger separations. The same approach could also be applied to calculations imposing periodic boundary conditions, provided that the correlation function decays to a value sufficiently close to zero for separations greater than half the system size. We show only the $q_\perp = \pi$ branch because the correlations are predominantly antiferromagnetic between the chains and the $q_\perp = 0$ branch is thus small and flat, with no interesting features. At half-filling ($\langle n \rangle = 1.0$), the Fourier transform $S(q, \pi)$ peaks at $q = \pi$ and has Lorentzian line shape, as one would expect for a spatially alternating, exponentially decaying function. As the system is doped, the peak shifts to smaller values of q commensurate with the lattice filling, so that it occurs at the "$2k_F$" wave vector $q^* = k_F^b + k_F^a = \langle n \rangle \pi$.

We have found that the finite-size effects for the charge and spin gaps can be large for a system with open boundary conditions, even on the largest lattice, 2×32 sites. We therefore must examine the gaps as a function of system size and extrapolate to the thermodynamic limit. We concentrate first on a particular filling, $\langle n \rangle = 0.875$, relatively close to half-filling. The charge gap Δ_c and the spin gap, Δ_s are plotted as a function of $1/L$ for three representative $t_\perp$ on lattice sizes up to 2×40 in Fig. 6. The charge gap, Fig. 6(a), scales approximately linearly with $1/L$ for all three values of $t_\perp$. The lines are least-squares fits to polynomials in $1/L$ whose order is chosen so that the number of free parameters is one less than the number of L points. The $1/L \rightarrow 0$ extrapolated value is zero to within the accuracy of the extrapolation in all three cases. We believe that this behavior is representative and that the charge gap vanishes for all $t_\perp$ and U at this filling. The spin gap, Fig. 6(b), shows different scaling behavior for $t_\perp = 0.5$, 1.0, and 2.0. For $t_\perp = 2.0$, the scaling is approximately linear in $1/L$ and the gap goes to zero in the thermodynamic limit. For $t_\perp = 1.0$, the $1/L^2$ term is substantial, and $\Delta_s(1/L \rightarrow 0) \approx 0.05$. For $t_\perp = 0.5$, the finite-size corrections are larger, the linear term in $1/L$ is large, and the $1/L^2$ coefficient is negative. Here $\Delta_s(0) \approx 0.02$, a small but finite value. However, the uncertainty is large because finite-size corrections are large and because the errors in Δ_s at $t_\perp = 0.5$ are relatively large. (In coupled chain systems, the accuracy of DMRG is generally inversely related to the coupling between chains.) Also shown
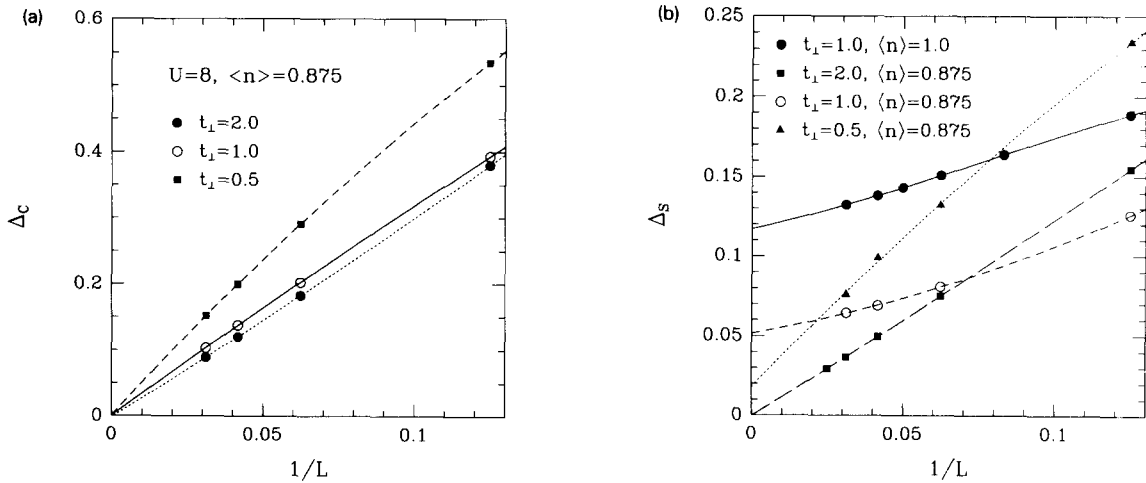
Fig. 6. (a) The charge gap Δ_c and (b) the spin gap Δ_s for $U = 8$ and $\langle n \rangle = 0.875$, as a function of the inverse chain length, $1/L$. The spin gap at half-filling is shown for comparison in (b), and the lines are least-squares fits of polynomials to the data, as explained in the text.
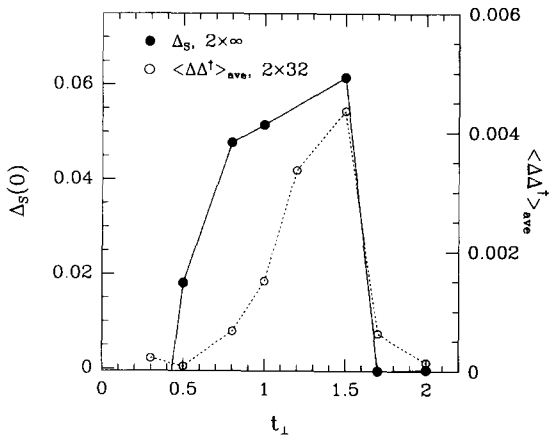

Fig. 7. The infinite system extrapolation of the spin gap, $\Delta_s(0)$, from Fig. 6(b) for $\langle n \rangle = 0.875$ and $U = 8$, and the average of the pair–pair correlation function $\langle \Delta(i)\Delta^\dagger(j) \rangle$ averaged between $|i - j| = 8$ and 12 lattice spacings.

for comparison is the spin gap for the half-filled system at $t_\perp = 1.0$, for which $\Delta_s(0) \approx 0.12$.

The extrapolated $1/L \to 0$ values of the spin gap, $\Delta_s(0)$, are shown plotted versus $t_\perp$ in Fig. 7. For $t_\perp > 1.7$, $\Delta_s(0) = 0$. For $U = 0$, the one band to two-band transition takes place at $t_\perp = 1.85$ at $\langle n \rangle = 0.875$. Within the BFRG picture [20], the system should be a one-band Luttinger liquid, i.e. have no spin gap and charge gap for $t_\perp > t_{\perp c}$. The BFRG also predicts some additional phases when $t_\perp$ is slightly below the band transition point where the Fermi velocities in

the two bands are very different, and at $t_\perp = t_{\perp c}$, when the antibonding band can no longer be treated by linearizing the Fermi surface. The additional phases below $t_{\perp c}$ have gapless spin and charge excitations, so the disappearance of the spin gap at a $t_\perp$ somewhat less than $t_{\perp c}$ is consistent with the existence of these phases, although we cannot distinguish between symmetric and antisymmetric spin and charge excited states within our DMRG calculation. We have, however, not yet seen any evidence for a reappearance of the spin gap exactly at $t_\perp = t_{\perp c}$.

The infinite system extrapolation of the spin gap, $\Delta_s(0)$, becomes zero at $t_\perp \approx 0.38$ and negative for smaller $t_\perp$, although Δ_s is positive for all the finite lattices we have examined. In addition, the nearest-neighbor spin–spin correlation $\langle M^z_{i,1} M^z_{i,2} \rangle$ goes to zero and has a discontinuity in slope at $t_\perp \approx 0.5$, as shown in Fig. 8. For $U = 0$, the bonding band is half-filled at $t_\perp = 0.4$, and the BFRG picture predicts that umklapp processes in the bonding band will become relevant at this point, leading to a C1S2 phase, consistent with a vanishing spin and charge gap. Therefore, the vanishing of $\Delta_s(0)$ at $t_\perp \approx 0.38$ could be associated with this weak-coupling feature.

For $t_\perp < 0.5$, the finite-size effects become large and the numerical accuracy of the DMRG procedure is reduced, so we have not been able to unambiguously determine whether or not the spin gap reappears in the small $t_\perp$ phase at this filling, as would be predicted
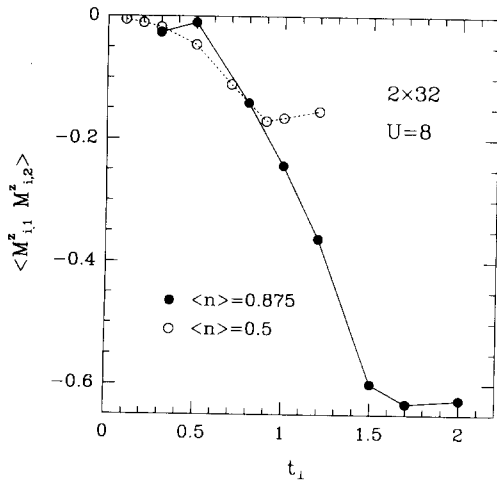
Fig. 8. The nearest-neighbor spin–spin correlation measured across a rung, $\langle M_{i,1}^z M_{i,2}^z \rangle$, at $\langle n \rangle = 0.875$ and $\langle n \rangle = 0.5$ as a function of $t_\perp$ for $U = 8$. Here we have chosen $i = 16$ on a 2×32 lattice.

by the BFRG.

For the quarter-filled system, the $U = 0$ one-band to two-band transition occurs at $t_\perp = 1.0$. For $t_\perp > 1.0$, the bonding band is half-filled, while for $t_\perp < 1.0$, both bands are fractionally filled. The BFRG predicts that within the one-band regime, the system will behave as a half-filled Luttinger liquid, i.e. a C0S1 phase, for which $\Delta_c \neq 0$ and $\Delta_s = 0$. We exhibit the charge and spin gaps as a function of $1/L$ in Fig. 9. For $t_\perp = 1.2$, $\Delta_c(0) \approx 0.08$, whereas $\Delta_s(0)$ vanishes to within the accuracy of the extrapolation. Since the finite-size effects are fairly large, we have studied lattice size up to 2×64. This is possible for $t_\perp = 1.2$ since the numerical accuracy is high at this parameter range, with a maximum discarded density-matrix weight of 6×10^{-7}, keeping 350 states on the 2×64 lattice. For $t_\perp = 0.7$, which is in the two-band region for $U = 0$, $\Delta_c(0)$ vanishes and $\Delta_s(0) \approx 0.07$. This behavior is consistent with the C1S0 phase predicted by BFRG in this region. In addition, since the bonding band is always less than half-filled for $t_\perp < t_{\perp c}$ at quarter filling, the BFRG calculation predicts no additional phases due to umklapp effects for small $t_\perp$. As can be seen in Fig. 8, the behavior of the spin–spin correlation across a rung, $\langle M_{i,1}^z M_{i,2}^z \rangle$, is smooth in the small $t_\perp$ region, unlike at $\langle n \rangle = 0.875$, consistent with the BFRG prediction.

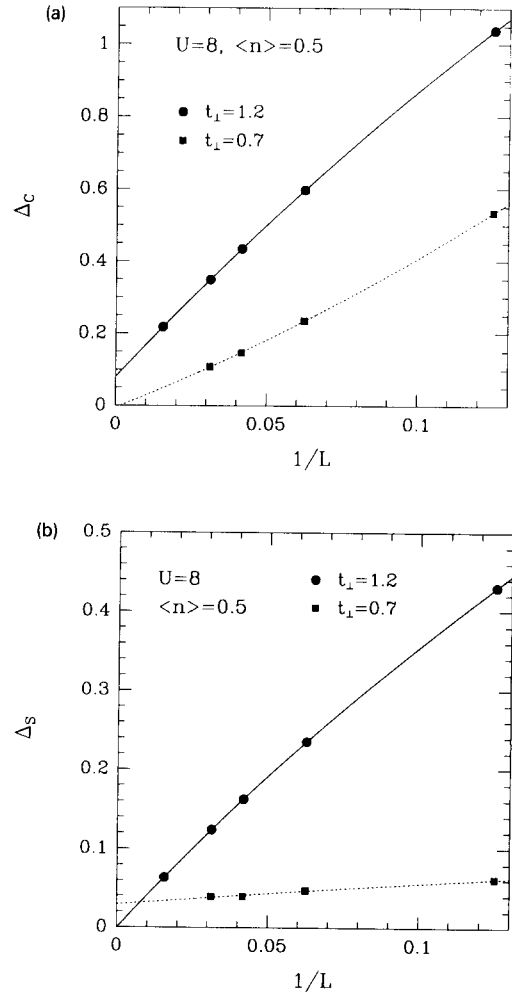We now concentrate on the doped spin gap phase (C1S0), present for isotropic $t_\perp$, and small to mod-

Fig. 9. (a) The charge gap Δ_c and (b) the spin gap, Δ_s, plotted as a function of $1/L$ for $U = 8$, $\langle n \rangle = 0.5$, and for $t_\perp = 1.2$ and 0.7.

erate doping. This phase could be relevant for the $La_{1-x}Sr_xCuO_{2.5}$ materials if, in fact, the ladders are sufficiently weakly coupled [31]. The general behavior of holes doped into a spin-liquid phase might also be relevant to the high-T_c materials. In particular, we are interested in whether there is an effective attractive potential between the holes, the nature of the state that they form, and the type of correlations dominant at long distances.

We first examine the local behavior as pairs of holes are doped into the system. In Fig. 10 we exhibit the local hole density $1 - \langle n_i \rangle$ plotted as a function of the rung index i. Since the system is symmetric with respect to exchange of the chains, we calculate the
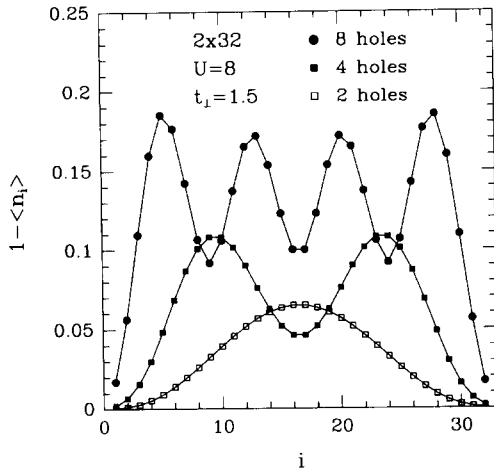
Fig. 10. The local hole density $1 - \langle n_i \rangle$ as a function of position along the chain i for 2, 4, and 8 holes ($\langle n \rangle = 0.96875, 0.9375, 0.875$) on a 2×32 chain for $U = 8$ and $t_\perp = 1.5$.

Fig. 11. The matrix element $\langle N_2 | (c_{r,\uparrow}^\dagger c_{r',\downarrow}^\dagger - c_{r,\downarrow}^\dagger c_{r',\uparrow}^\dagger) | N_1 \rangle$ of the pair creation operator between a state $|N_1\rangle$ with two holes and $|N_2\rangle$ with four holes on a 2×16 lattice with $U = 8$ and $t_\perp = 1.0$. The distance ℓ is the rung separation $|i - j|$ for intrachain part and $|i - j| + 1$ for the cross-chain part.

average value on a rung. The inhomogeneous structure is due to the open boundary conditions as well as the interaction between the holes. Due to kinetic-energy effects, the boundaries repel the holes. When two holes are put into the system, as can be seen in Fig. 10, the hole density has one peak with a maximum at the center of the ladder. In other words, the holes tend to both be near the same rung of the ladder, indicating a net attraction between the holes. We have calculated the pair binding energy of two holes in a half-filled $2 \times L$ lattice, defined as

$$E_b = 2E_0(L, L - 1)$$
$$-E_0(L, L) - E_0(L - 1, L - 1) \qquad (9)$$

on a 2×32 lattice with $t_\perp = 1.0$, and obtain a positive binding energy, $E_b \approx 0.14$. As more holes are added to the system, the number of peaks in the hole density is equal to the number of hole pairs, indicating that there is a tendency for the hole pairs to repel one another.

In order to understand further the nature of the interaction between holes in the antiferromagnetic spin liquid, we have examined the pair wave function of two holes directly. We do this by calculating the matrix element of the pair creation operator,

$$\langle N_2 | \Delta_{rr'}^\dagger | N_1 \rangle = \langle N_2 | (c_{r,\uparrow}^\dagger c_{r',\downarrow}^\dagger - c_{r,\downarrow}^\dagger c_{r',\uparrow}^\dagger) | N_1 \rangle, \qquad (10)$$
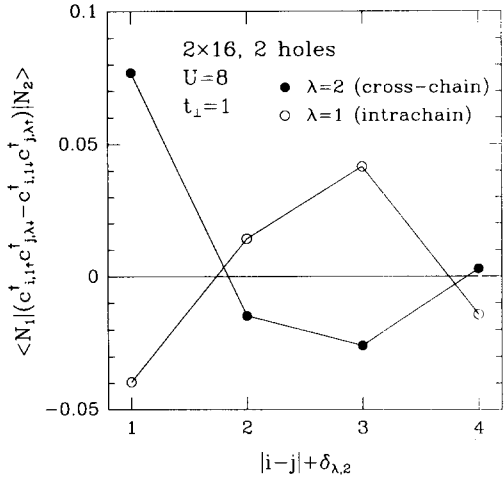
between a state $|N_1\rangle$ with N spin-up and N spin-down electrons, and a state $|N_2\rangle$ with $N - 1$ spin up and $N - 1$ spin down electrons. Here the index $r = (i, \lambda)$ denotes the position. The pair wave function can then be extracted by examining the dependence of this matrix element on $(r - r')$. The result for the matrix element between the state with four holes ($|N_1\rangle$) and the state with two holes ($|N_2\rangle$) at $t_\perp = 1$ ($N = 14$ on a 2×16 lattice) is shown in Fig. 11. The distance along the ordinate is the rung separation plus the cross–chain distance (0 or 1), so that a value of 1 corresponds to nearest-neighbor points either along or between the chains, and subsequent points are further along the chains. We have also averaged the matrix element for a number of site pairs with the same $(r - r')$ in order to reduce the finite-size effects due to the open boundaries.

As can be seen in the plot, the largest amplitude for the pair matrix element is for a nearest-neighbor site across a rung, and the second largest for a nearest-neighbor site on the same chain. The two amplitudes have opposite signs, indicating a d wave-like symmetry. The d wave-like structure of the pair wave function is maintained as the separation is increased along the chain. In addition, the amplitude is strongly suppressed when the two particles are created on sites on the same sublattices, as can be seen by the smaller amplitude at

every other point. This structure can be understood in a strong-coupling picture by considering a dimer RVB state [23], which gives a good qualitative description of the two-chain Heisenberg system. Here, we have added two holes to a half-filled system that is close to the Heisenberg limit. When two holes are added on the same sublattice within the dimer RVB state, the RVB state is frustrated in that the number of possible valence bond configurations is greatly reduced, leading to a higher energy. Therefore, the amplitude of the state in which both holes are on the same sublattice is suppressed in order to minimize the probability of the system being in such a configuration.

We have also examined the pair wave function by calculating similar matrix elements for $t_\perp = 2.0$ and $t_\perp = 0.3$ in order to examine the large $t_\perp$ Luttinger liquid (C1S1) phase and the small $t_\perp$ phase. We find that the pair wave function does not maintain the coherent structure shown in Fig. 11 for separations larger than the nearest-neighbor separations, indicating that this structure is only present in the C1S0 part of the phase diagram.

We have now ascertained that there is a tendency towards pairing within the doped, spin-gap phase (C1S0), and have examined the shape of the pair wave function. However, in order to determine the nature of the ground state, particularly with a view towards possible ordering via three-dimensional crossover in the real materials, we must examine the long-distance behavior of the correlation functions. We choose a pairing order parameter that creates a pair locally in real space, but has a large overlap with the actual pair wave function:

$$\Delta^\dagger(i) = c^\dagger_{i,1,\uparrow} c^\dagger_{i,2\downarrow} - c^\dagger_{i,1,\downarrow} c^\dagger_{i,2\uparrow}. \quad (11)$$

This operator creates a pair in a spin singlet on two neighboring sites on a rung (labeled i). We then cal-
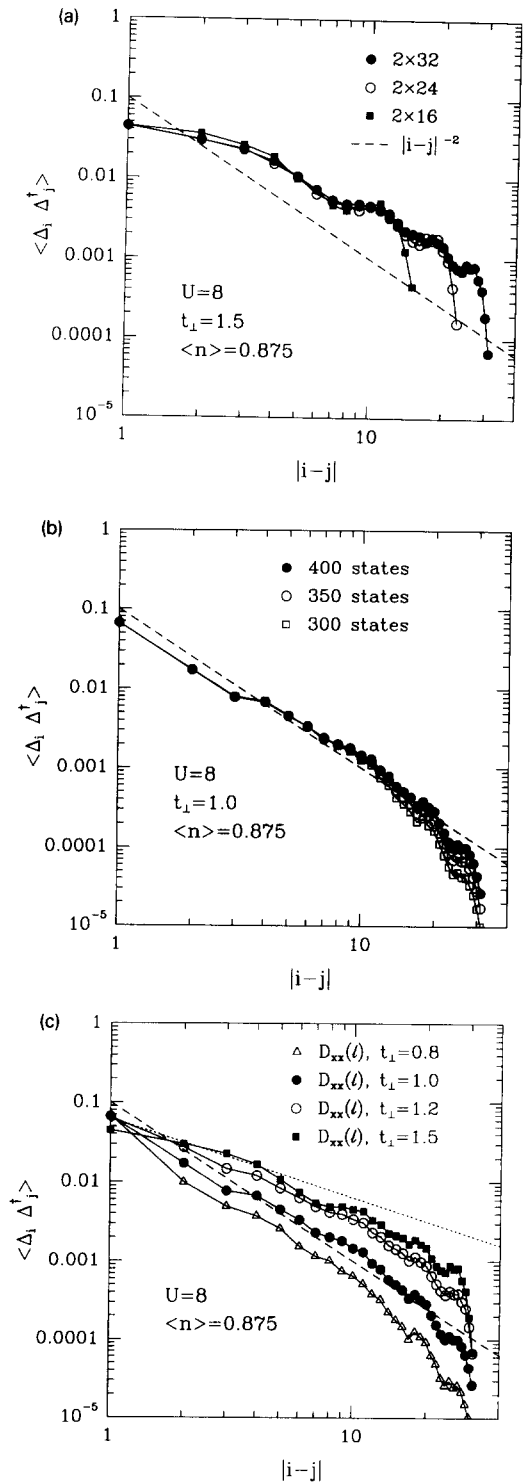
Fig. 12. The pair–pair correlation function $\langle \Delta(i)\Delta^\dagger(j)\rangle$ plotted on a log–log scale for for $U = 8$ and $\langle n \rangle = 0.875$. In (a) the $t_\perp = 1.5$ susceptibility is plotted for different system sizes, in (b) the $t_\perp = 1.0$ susceptibility is plotted for different numbers of states kept in the DMRG procedure on a 2 × 32 lattice, and in (c) the susceptibility is plotted for various $t_\perp$ on a 2 × 32 lattice. The dashed line gives the $|i - j|^{-2}$ decay of the $U = 0$ pair susceptibility, and the short dashed line in (c) shows a decay of $|i - j|^{-1}$.

culate the corresponding pair correlation function, $\langle \Delta(i) \Delta^\dagger(j) \rangle$, as a function of distance between the rungs, $|i - j|$. This pair correlation is shown, plotted on a log–log scale for various system sizes and $t_\perp$ values within the spin-gapped phase at $\langle n \rangle = 0.875$ in Fig. 12.

In order to exhibit the finite-size effects, we show the pair correlation function on 2×8, 2×16, and 2×32 lattices in Fig. 12(a). Recall that the local density, as seen in Fig. 10, can have substantial dependence on lattice position. Since the correlation functions on the finite lattice with open boundaries are not translationally invariant, we must choose one or more i, j pairs in order to best approximate infinite system behavior. Originally, we calculated the correlation functions by choosing one i, j pair for each $|i - j|$ so that the pair was as symmetrical about the center of the lattice as possible. For odd separations, i and j can be chosen symmetrically about the lattice center (for a lattice of even length), whereas for even separations, they cannot be. Such an odd–even effect produced, for example, a spurious peak at $q = (\pi, \pi)$ in the Fourier transform of the spin–spin correlation function for the doped system (shown in Fig. 5). In general, correlation functions in real space calculated in this way show spurious oscillations which can be seen by comparing the correlation functions at a given distance on different lattice sizes. In order to try to remove these effects, we average correlation functions over a number of i, j pairs for each $|i - j|$. We have found it best to take enough pairs so that one averages over the wavelength of the oscillations in the local quantities. Here we average over six pairs, starting with the symmetrically placed pair and then proceeding down the lattice. When $|i - j|$ gets near the lattice size, the number of possible i, j pairs is smaller due to the proximity to the boundaries. As seen in Fig. 12(a), the pair correlation function treated in this way shows only small finite-size effects until the last few points before the boundary are reached. There are oscillations remaining in the correlation function, but these are not a finite-size effects and are present in the thermodynamic limit. The unphysical peaks at $q = (\pi, \pi)$ for the doped cases in Fig. 5 disappeared after this averaging procedure was applied to $S(i, j, \lambda)$.

Another potential source of inaccuracy in the calculation of correlation functions is the error introduced by the truncation of states within the DMRG proce-

dure. While the errors in the energies of the ground and low-lying excited states are correlated with the total weight of the discarded density-matrix eigenvalues, as discussed above, the accuracy of the correlation functions, especially at long distances, is somewhat harder to estimate. One can, however, examine the change in the correlation function with the number of states kept in the DMRG procedure. We exhibit in Fig. 12(b) the pair–pair correlation function plotted for 300, 350, and 400 states kept for the system block. We estimate the errors to be within the symbol size for all but the largest few separations, for which the logarithmic scale amplifies small absolute errors in the correlation function. (Since the DMRG procedure is more accurate for larger $t_\perp$, $t_\perp = 1.0$ is typical or worse for the curves shown in Fig. 12(c).)

In Fig. 12(c), we plot the pair correlation function $\langle \Delta(i) \Delta^\dagger(j) \rangle$ on a log–log scale as a function of $|i - j|$ on a 2×32 lattice for a variety of $t_\perp$ values within the C1S0 phase at $\langle n \rangle = 0.875$. Also shown on the plot are lines representing the power law decays $|i - j|^{-1}$ and $|i - j|^{-2}$. As can be seen, the pair correlation functions are approximately straight lines on the log–log scale, implying a power-law decay of the correlations. If this power law has the form $|i - j|^{-\nu}$, ν ranges from slightly greater than 2 for $t_\perp = 0.8$ to approximately 1 for $t_\perp = 1.5$. In the noninteracting, $U = 0$, system, the pairing correlation function decays as $|i - j|^{-2}$, so the pairing is only enhanced over that in the noninteracting system for $t_\perp > 1.0$. The strength of the pairing correlations is correlated with the size of the spin gap, as shown in Fig. 7. The average strength of the pair correlation function, calculated by averaging $\langle \Delta(i) \Delta^\dagger(j) \rangle$ between $|i - j| = 8$ and $|i - j| = 12$ lattice spacings, is shown as a dashed line. In the isotropic case, the pairing exponent $\nu \approx 2$. Since this phase is predicted to be a C1S0 phase by the BFRG, we would expect $\nu = 1/K_\rho$ within a Luther–Emery picture. Recall that the weakest criterium for dominant pair correlations within a Luther–Emery picture is that $K_\rho > 1$, i.e. that $\nu < 1$. Therefore, the pairing correlations would not be dominant for the isotropic system within a Luther–Emery picture, and a direct application of this model to the $La_{1-x}Sr_x CuO_{2.5}$ materials would not predict a superconducting ground state.

We now search for a CDW correlation function with a reciprocal behavior to the pairing correlations, as in Eq. 5. In Fig. 13, we plot the continuous Fourier
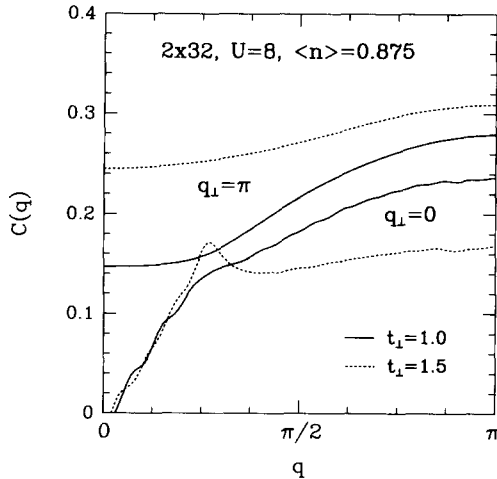
Fig. 13. The continuous Fourier transform of the density–density correlation function $C(q)$ on a 2×32 lattice with $U = 8$ and $\langle n \rangle = 0.875$ for $t_\perp = 1.0$ and $t_\perp = 1.5$. The upper curves are the $q_\perp = \pi$ branches and the lower curves the $q_\perp = 0$ branches.

transform of the CDW correlation function

$$C(i, j, \lambda) = \langle n_{i,\lambda} n_{j,1} \rangle - \langle n_{i,\lambda} \rangle \langle n_{i,1} \rangle \qquad (12)$$

at $\langle n \rangle = 0.875$, for $t_\perp = 1.0$ and $t_\perp = 1.5$, within the C1S0 spin-liquid phase. The real-space correlation function is averaged and Fourier transformed in the same way as the spin–spin correlation function of Eq. 6. As can be seen, there is no distinct peak at the "$2k_F$" wave vector $q = (q^*, \pi)$, where $q^* = k_F^b + k_F^a = \pi \langle n \rangle$. However, there is a peak at $q = (\pi/4, 0)$ which grows and sharpens with increasing $t_\perp$. This wavevector is the correct value for the "$4k_F$" CDW correlations, for which $|2(k_F^b + k_F^a) \bmod 2\pi| = \pi/4$. Within a bosonization treatment [21,20], the "$4k_F$" peak should not appear in the density–density correlation function of Eq. 12, but only in a density–density correlation function composed of four fermion densities. We believe that the fact that it appears in $C(q)$ is due to the band curvature, which is not included in the bosonization picture, and effectively includes higher-order density–density correlations in $C(q)$.

We have isolated the "$4k_F$" portion of the density–density correlation function by calculating the correlation function of a simple effective rung density

$$n_i^{\text{eff}} = n_{i,1\uparrow} n_{i,2\downarrow}. \qquad (13)$$

Since n_i^{eff} is composed of four fermion operators, rather than two as in the ordinary density–density

correlation function, in order to form the correlation function, $\langle n_i^{\text{eff}} n_j^{\text{eff}} \rangle$ one must subtract off fourteen different disconnected pieces, not only $\langle n_i^{\text{eff}} \rangle \langle n_j^{\text{eff}} \rangle$, as in Eq. 12. We will not write all the disconnected terms explicitly here. However, the subtraction can be carried out to obtain the real-space correlation function $N(i, j)$ which can be averaged over a number of i, j pairs and Fourier transformed with respect to the rung index, as was done for the spin–spin and density–density correlation functions above, to obtain $N(q)$. The Fourier transformed rung-density correlation function $N(q)$ is plotted for $t_\perp = 1.0$ and $t_\perp = 1.5$ in Fig. 14(a). As can be seen, the "$4k_F$" peak at $q = \pi/4$ is now well-defined, and the broad background seen in $C(q)$ is no longer present. As in Fig. 13, the peak at $q = \pi/4$ grows in size and sharpness as $t_\perp$ is increased from 1.0 to 1.5. In Fig. 14(b) we exhibit the averaged real-space correlation function $N(\ell)$, where $\ell = |i - j|$, on a log–log scale in order to estimate the exponent of the decay. The envelope of the correlations is consistent with a straight line on the log–log scale and therefore an algebraic decay, although the "$4k_F$" structure makes it difficult to directly determine how the envelope decays. If we assume a form $|i - j|^{-\gamma}$ for the decay of the envelope, one can estimate γ to be slightly greater than 2 for $t_\perp = 1.0$, and slightly less than 2 for $t_\perp = 1.5$.

Therefore, the behavior is opposite to what one would expect from the Luther–Emery model: both the pairing exponent ν and the "$4k_F$" CDW exponent γ decrease as $t_\perp$ increases within the doped spin-liquid phase, and clearly do not obey the relationship $\nu\gamma = 1$. It is not clear why the exponents do not behave as expected. One possibility is that the identification of this phase with the Luther–Emery-like phase found in the bosonization calculations is incorrect. Another possibility is that there is another CDW-like correlation function that behaves in the expected way. A fact that could also be important is that the CDW should be quite slowly decaying. For example, in the isotropic case, $\nu \approx 2$ so that γ should be $\approx \frac{1}{2}$. Perhaps such long-range CDW correlations effectively put the system into an ordered CDW state on a finite lattice with open boundaries. In this case, the "$4k_F$" CDW correlation function, which measures the decay of the fluctuations, might not behave in the expected way.

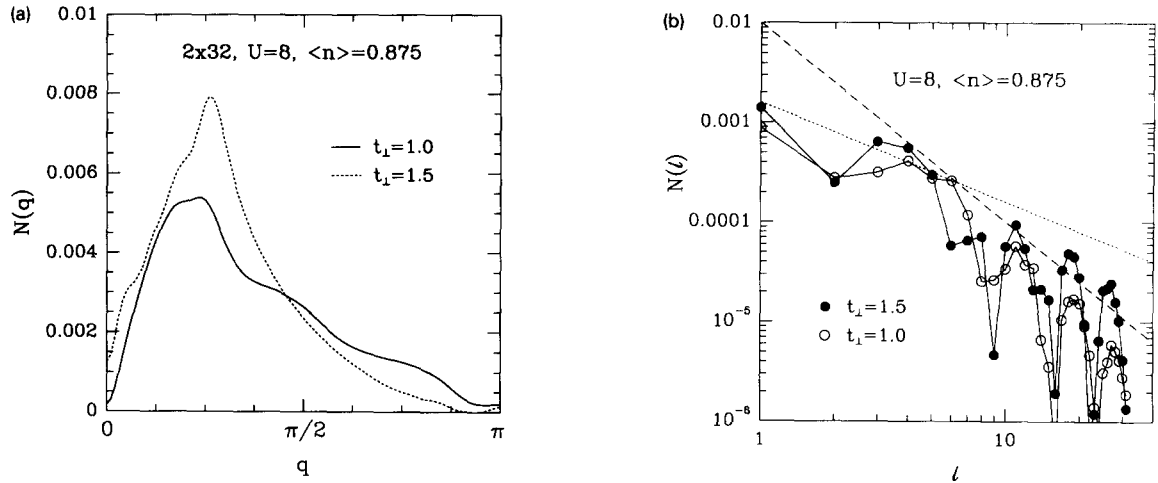Fig. 14. The $4k_F$ density–density correlation function $N(i,j)$, as defined in Eq. (13), (a) Fourier transformed and (b) in real space on a 2×32 lattice for $U = 8$, $\langle n \rangle = 0.875$, and $t_\perp = 1.0$, 1.5.

3. Conclusion

We have explored the ground-state phase diagram of the two-leg Hubbard ladder as a function of the band filling $\langle n \rangle$ and the interchain hopping matrix element $t_\perp$, concentrating on the case of intermediate to strong on-site interaction, primarily $U = 8$. For the half-filled system, we find a spin-gapped insulating phase for all $t_\perp$ and U accessible to our numerical density-matrix renormalization group calculations. For weak U, there is a relatively sharp transition from a spin-liquid insulator at small $t_\perp$ to a band insulator for $t_\perp > 2.0$. As U is increased, this transition becomes a gradual crossover more consistent with a Heisenberg-model picture. However, at large enough $t_\perp$, we would expect a return to a band insulator for all finite U. This behavior is consistent with recent weak-coupling renormalization group and bosonization calculations [20], as well as, in the large U limit, strong-coupling Heisenberg model calculations [22,11].

When the half-filled insulator is doped with holes, we find a number of distinct phases. The major feature dominating the phase diagram is associated with the weak-coupling one-band to two-band transition. For $t_\perp$ larger than the $U = 0$ band transition value, $t_{\perp c}$, our numerical results show a behavior consistent with that of a Luttinger liquid, whose band filling corresponds to the filling of the $U = 0$ bonding band. The development of a charge gap, expected in the half-filled

Luttinger liquid, clearly occurs at quarter filling in the two-leg ladder for $t_\perp > t_{\perp c}$. For $t_\perp < t_{\perp c}$, there is a region near $t_{\perp c}$ in which the spin gap still vanishes. This is consistent with a weak-coupling renormalization group (RG) calculation of Balents and Fisher [20], which predicts phases with gapless spin excitations where the bands overlap, but the Fermi velocities are very different. In addition, for light doping and small $t_\perp$, we find the spin gap vanishes at a finite $t_\perp$ consistent with a half-filled bonding band, a point at which the Balents–Fisher calculation predicts a phase with a vanishing spin gap associated with umklapp processes in the half-filled bonding band. For the remainder of the $t_\perp < t_{\perp c}$ region, and especially in the light of a moderately doped isotropic case there is a spin-gapped phase with gapless charge excitations in which there are algebraically decaying d wave-like superconducting correlations, and "$4k_F$" CDW correlations. However, the pairing correlations do not seem to be dominant in the isotropic system, and exponents of the CDW and pairing correlations do not seem to obey the inverse relationship predicted by a bosonization picture [21,20].

Acknowledgements

References

[1] Z. Hiroi, M. Azuma, M. Takano and Y. Bando, J. Solid State Chem. 95 (1991) 230.

[2] R.J. Cava et al., J. Solid State Chem. 94 (1991) 170.

[3] R. Norrestam, M. Nygrew and J.O. Bovin, Angew. Chem. Intl. Ed. Engl. 30 (1991) 864.

[4] D.C. Johnston et al., Phys. Rev. B 35 (1987) 219.

[5] M. Azuma et al., Phys. Rev. Lett. 73 (1994) 3463.

[6] Z. Hiroi and M. Takano, Nature (London) 377 (1995) 41.

[7] S.R. White, Phys. Rev. Lett. 69 (1992) 2863;
idem, Phys. Rev. B 48 (1993) 10345.

[8] R.M. Noack, S.R. White and D.J. Scalapino, Phys. Rev. Lett. 73 (1994) 882;
idem, Europhys. Lett. 30 (3) (1995) 163.

[9] E. Dagotto and T.M. Rice, Science 271 (1996) 618.

[10] E. Dagotto, J. Riera and D.J. Scalapino, Phys. Rev. B 45 (1992) 5744.

[11] T. Barnes et al., Phys. Rev. B 47 (1993) 3196;
T. Barnes and J. Riera, Phys. Rev. B 50 (1994) 6817;
R.S. Eccleston, T. Barnes, J. Brody and J.W. Johnson, Phys. Rev. Lett. 73 (1994) 2626.

[12] T.M. Rice, S. Gopalan and M. Sigrist, Europhys. Lett. 23 (1993) 445.

[13] H. Tsunetsugu, M. Troyer and T.M. Rice, Phys. Rev. B 49 (1994) 16078;
M. Troyer, H. Tsunetsugu and T.M. Rice, Phys. Rev. B 53 (1996) 251.

[14] H. Endres, et al. Phys. Rev. B 53 (1996) 5530.

[15] C.M. Varma and A. Zawadowski, Phys. Rev. B 32 (1985) 7399.

[16] H.J. Schulz, Int. J. Mod. Phys. B 5 (1991) 57.

[17] A.M. Finkel'stein and A.I. Larkin, Phys. Rev. B 47 (1993) 10461.

[18] M. Fabrizio, A. Parola and E. Tosatti, Phys. Rev. B 46 (1992) 3159;
M. Fabrizio, Phys. Rev. B 48 (1993) 15838.

[19] D.V. Khveshchenko and T.M. Rice, Phys. Rev. B 50 (1994) 252;
D.V. Khveshchenko, Phys. Rev. B 50 (1994) 380.

[20] L. Balents and M.P.A. Fisher, Phys. Rev. B 53 (1996) 12133.

[21] N. Nagaosa and M. Oshikawa (unpublished) cond-mat/9412003;
N. Nagaosa, Solid State Comm. 94 (1995) 495.

[22] Sudha Gopalan, T.M. Rice and M. Sigrist, Phys. Rev. B 49 (1994) 8901.

[23] S.R. White, R.M. Noack and D.J. Scalapino, Phys. Rev. Lett. 73 (1994) 886.

[24] S. Liang, B. Douçot and P.W. Anderson, Phys. Rev. Lett. 61 (1988) 365.

[25] D. Poilblanc, D.J. Scalapino and W. Hanke, Phys. Rev. B 52 (1995) 6796.

[26] F.D.M. Haldane, Phys. Rev. Lett. 45 (1980) 1358;
idem, J. Phys. C 14 (1981) 2585.

[27] C.N. Yang and C.P. Yang, Phys. Rev. 150 (1966) 321; ibid., 150 (1966) 327.

[28] A. Luther and V.J. Emery, Phys. Rev. Lett. 33 (1974) 589;
V.J. Emery, in: Highly Conducting One-Dimensional Solids, eds. J.T. Devreese et al. (Plenum, New York, 1979).

[29] T. Giamarchi and H.J. Schulz, Phys. Rev. B 32 (1988) 7399.

[30] M. Azzouz, L. Chen and S. Moukouri, Phys. Rev. B 50 (1994) 6233.

[31] Recent bandstructure calculations by L.F. Mattheiss, Solid State Commun. 97 (1996) 751, suggest that $La_{1-x}Sr_xCuO_{2.5}$ could be rather three-dimensional.